A study by response surface methodology (RSM) on optimization of phosphorus adsorption with nano spherical calcium carbonate derived from waste

Shuo Deng and Yinguang Chen

ABSTRACT

A nano spherical $CaCO_3$ (NSC) derived from solid waste (precipitated from tris(α-chloropropyl) phosphate and triethyl phosphate mixed wastewater) was prepared as adsorbent for phosphorus removal from aqueous solution. Response surface methodology (RSM) was used to develop an approach for the evaluation of phosphorus adsorption process, and Box-Behnken design was performed to investigate the effects of various experimental parameters (temperature, contact time, initial pH and dosage of absorbent) on phosphorus adsorption. The model results of experimental data gave a high correlation coefficient ($R^2 = 0.9658$), and a predictive model of quadratic polynomial regression equation and optimum level values were established successfully. It was found that the adsorption efficiency and adsorption capacity reached 97.05% and 123.79 mg/g, respectively, under conditions of temperature of 45 °C, initial pH 5.3, contact time of 11 h, and absorbent amount of 392 mg/L. X-ray diffraction (XRD) analysis testified new phase, $Ca_{10}(PO4)_6CO_3$, was produced in the adsorption process. Apart from that, adsorption behavior fitted well with the Langmuir isotherm model and logistic growth model. The thermodynamic study indicated that phosphorus removal by NSC as adsorbent was a spontaneous, endothermic, and mainly chemical adsorption process.

Key words | adsorption, nano calcium carbonate, phosphate removal, phosphorus, response surface method

Shuo Deng
Yinguang Chen (corresponding author)
State Key Laboratory of Pollution Control and Resources Reuse, School of Environmental Science and Engineering,
Tongji University,
1239 Siping Road, Shanghai 200092,
China
E-mail: *yinguangchen@tongji.edu.cn*

INTRODUCTION

The release of phosphorus from municipal wastewater, industrial discard solution, agricultural areas runoff and landfill leachate often cause water pollution. Excessive phosphate in water body can cause abnormal growth of microorganisms and algae, which will deteriorate the water quality and eventually lead to eutrophication (Yu *et al.* 2017). Therefore, although phosphorus is a necessary element for biological growth, its concentration in water must be limited to a reasonable value (Choi *et al.* 2016). Various approaches had been developed for the removal of phosphate from water, including chemical precipitation, adsorption, biological removal, reverse osmosis, membrane and ion exchange, among them, biological removal, chemical precipitation and adsorption are the most common methods. Biological phosphorus removal is a low-cost and environmentally friendly method, but microorganisms are very sensitive to the requirements of water quality, and the change of operating conditions will have a great effect on the adsorption effect (Diamadopoulos *et al.* 2007). Chemical precipitation is usually used to remove phosphorus by adding metal ions, such as Al^{3+}, Fe^{2+}/Fe^{3+} and Mg^{2+}, which will consume a lot of coagulants and produce a large amount of unmanageable sludge (Ahmad *et al.* 2016). The removal of phosphate from water by adsorption has attracted much attention due to its advantages of low cost, simple operation and less sludge output (Ko *et al.* 2016).

Recently, metallic oxide and hydroxide materials, such as alumina, Fe-Al binary oxide (Tofik *et al.* 2016), cobalt hydroxide (Zolgharnein *et al.* 2017) with nanostructures have gained special attention in adsorption due to small particle size, large specific surface area, high *in situ* reactivity and weak diffusion resistance. Moreover, at a relatively low value of pH, the surface protonation of these kinds of nanoscale adsorbents will be enhanced. Increased

doi: 10.2166/wst.2019.048

protonation would increase the positively charged sites, enlarging the attraction force existing between the sorbent surface and the negatively charged (PO_4^{2-}, HPO_4^- and $H_2PO_4^-$) anions, which lead adsorption of phosphate (Tofik *et al.* 2016; Zolgharnein *et al.* 2017). In other studies, calcium was used to decorate sludge derived carbon (Kong *et al.* 2018), clad clinoptilolite (Zhou *et al.* 2017) and synthesize hydrocalumite (Oladoja *et al.* 2014) to enhance the adsorption capacity. Because the release of Ca^{2+} in aqueous solution precipitated phosphate on the surface of the adsorbent and, of course, environmental friendliness of calcium is also the reason to be chosen. The surface of $CaCO_3$ has positively charged sites to attract negative ions in the case of pH < 8 (Somasundaran & Agar 1967) and obviously, $CaCO_3$ has a large proportion of calcium itself. There are some reports of natural calcite for phosphate removal, but the research on the synthesis of nano $CaCO_3$ has not received much attention. An experiment confirmed that removal rate of phosphate (concentration of phosphorus is 50 mg/L) by nano $CaCO_3$ reached 98% at the condition of room temperature, initial pH 12, contact time of 30 min and absorbent amount of 20 g/L, of which the adsorption capacity was 2.45 mg/g (Cheng & Xie 2008). Adsorption isotherms and kinetics were studied in aforementioned phosphorus adsorption studies. Langmuir and Freundlich models are common adsorption isotherms and, in these papers, adsorption processes conformed to Langmuir isotherm (Cheng & Xie 2008; Oladoja *et al.* 2014; Zolgharnein *et al.* 2017; Kong *et al.* 2018), which means that these materials are monolayer adsorption (Liu *et al.* 2016). In the above papers, the kinetic parameters for the sorption of phosphate onto the different materials were obtained by fitting the time–concentration profile data to the pseudo-first-order and pseudo-second-order kinetic models, and the results showed that the pseudo-second-order gave the best description of the sorption process (Oladoja *et al.* 2014; Tofik *et al.* 2016; Zhou *et al.* 2017; Zolgharnein *et al.* 2017; Kong *et al.* 2018). Of course, the adsorption model is not fixed, which depends on the properties of adsorption materials. For example, the process of phosphorus adsorption was also well described by Freundlich isotherm (Tofik *et al.* 2016) and power function model (Yu *et al.* 2017).

After catalytic oxidation of tris(α-chlorophyll) phosphate and triethyl phosphate wastewater from a chemical plant, 50 mg/L phosphate-P was found in the water. In order to remove this phosphorus, $CaCl_2$ and Na_2CO_3 were added to the water, resulting in a large number of calcium containing solid wastes (CSW). In the present study, nano $CaCO_3$ powder was prepared from CSW and its removal conditions were further investigated, which improved adsorption capacity from 2.45 mg P/g $CaCO_3$ to 123.79 mg P/g $CaCO_3$.

METHODS

The preparation of the adsorbent

All chemical reagents are of analytical grade. The CSW (components were listed in Table 1) was washed with deionized water and then oven-dried at 105 °C to constant weight. The CSW was dissolved by 4 M HCl with a dosage of 2.4 mL/g, and the obtained solution was added with 20% $Ca(OH)_2$ suspension until the pH was 10 to precipitate Al^{3+}, Fe^{3+}, Mg^{2+} and PO_4^{3-}. After centrifugal separation of the precipitates, solution pH was adjusted to 6.5 with 1 M HCl to convert excessive $Ca(OH)_2$ to $CaCl_2$. The $CaCl_2$ solution was diluted to 0.3 mol/L and sealed for the next experiment. Nano spherical calcium carbonate (NSC) was synthesized according to the following procedure (Fang & Shen 2002). First, 0.3 g ethylenediaminetetraacetic acid (EDTA) was added into a 250 mL of 0.3 mol/L Na_2CO_3 solution, under stirring at speed of 800 rpm. 250 mL of 0.3 mol/L $CaCl_2$ solution dropped into the above solution within 5 min and then, 0.3 g Na_2HPO_4 was added into the mixed solution. The mixture was stirred continuously for 15 min at 10 °C in biochemistry cultivation cabinet (SPX-150SHII, China) and then it was separated by centrifuge (LXJ-IIB, China) and washed with deionized water. After that, the solid was oven-dried at 105 °C. Finally, the NSC was ground and sealed for further experiments.

Batch adsorption experiments

$NaH_2PO_4{\cdot}2H_2O$ was used to prepare the stock solution containing 1,000 mg/L of phosphorus, which was further diluted with deionized water to the desired initial concentrations. Batch adsorption studies were performed for phosphorus removal by NSC in 250 mL glass flasks. 300–400 mg/L of NSC was added into 100 mL of phosphorus solution with the known concentration (C_0) ranged between

Table 1 | Components of calcium containing solid wastes (CSW)

Component	CaO	Al_2O_3	Fe_2O_3	MgO	P_2O_5	SiO_2	H_2O
Content (%)	11.9	1.9	1.3	2.0	2.9	5.2	61.9

20 and 60 (mg/L). Initial pH of the solution was adjusted by 2 M HCl and 2 M NaOH solutions. The glass flasks were covered with plastic film and then set on the magnetic stirring water-bath (FJS-6, China) with constant temperature (30–50 °C) and agitated at a constant rate (500 rpm) for different hours. Adsorption isotherm studies were conducted by varying the initial phosphorus concentration (20–60 mg/L) at several different temperatures (30, 40 and 50 °C). Parameter absorption time was ranged from 1 h to 10 h at 40 °C for the studies of adsorption kinetics. The amount of adsorbed phosphorus (q) and adsorption rate (R) onto NSC were calculated with the Equations (1) and (2), respectively, where q is the phosphorus uptake (mg phosphorus/g of sorbent), R is the adsorption rate (%), C_0 and C_e is the initial and final of concentration phosphorus in solution (mg/L), V is total solution volume (mL), and m is the amount of the sorbent (mg):

$$q = (C_0 - C_e)V/m \tag{1}$$

$$R = (C_0 - C_e)/C_0 \times 100\% \tag{2}$$

Analytical method

Phosphorus analysis was carried out with a UV–vis spectrophotometer (UV-1800, Japan) using the molybdenum antimony method at 700 nm. Solution pH was monitored with a standard pH meter (6010 M, China). The morphological characterization of LECA was determined by scanning electron microscope and transmission electron microscope. X-ray diffraction (XRD; D8 ADVANCE, Germany) was used to determine the structure and composition of adsorbents. Phase identification was performed using XRD data analysis software and its powder diffraction file (PDF) database (Jade 6.0). Response surface methodology was used to determine the optimum condition for the phosphorus removal, while in the conventional method, the accomplishment of the experiments using conventional method and investigation of interaction between parameters is very time consuming and impractical. The surface is usually fitted by quadratic equation and the phosphorus adsorption rate (response, y) dependency to all variables can be represented as Equation (3) (Shojaeimehr *et al.* 2014), where y is the response, b_0, b_i, b_{ij}, b_{ii} are the regression coefficients of variables for intercept, linear, interaction terms and quadratic, respectively. X_i and X_j are the independent variables and ε is the residual term.

$$y = b_0 + \sum_{i=1}^{4} b_i X_i + \sum_{i=1}^{4}\sum_{j=1}^{4} b_{ij} X_i X_j + \sum_{i=1}^{4} b_{ii} X_i^2 + \varepsilon \tag{3}$$

RESULTS AND DISCUSSION

Characteristics of the adsorbent

The morphology of NSC surface in magnification is indicated in Figure 1(a) and 1(b). It implies that NSC was spherical in shape and the particle size was mainly

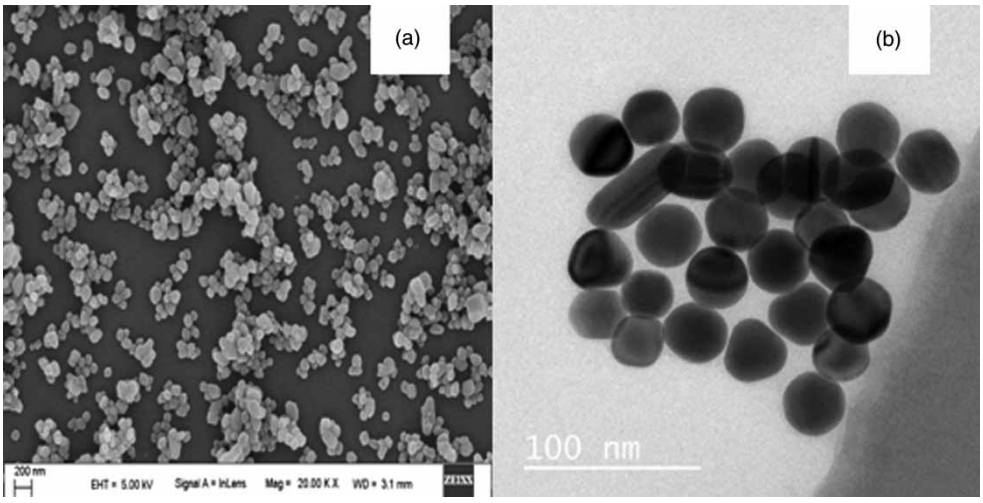

Figure 1 | SEM, TEM and XRD analysis of NSC: (a) SEM of NSC before adsorption; (b) TEM of NSC before adsorption.

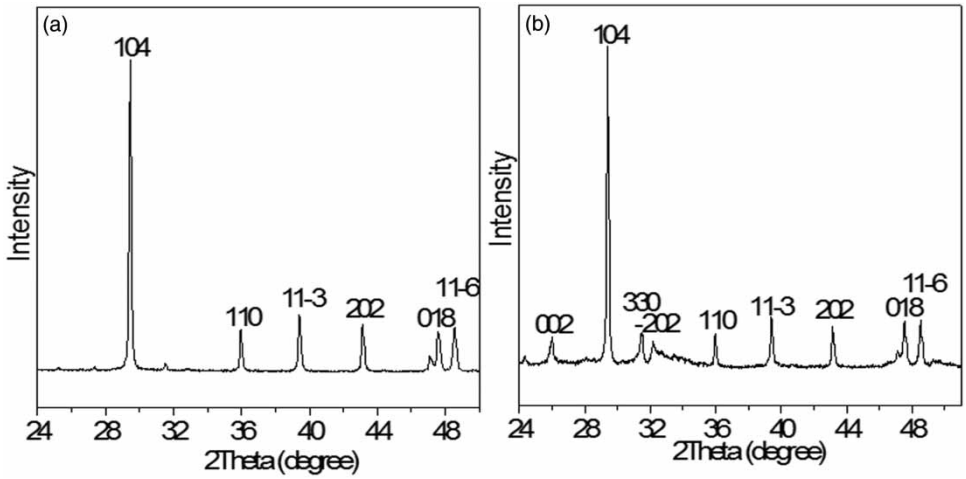

Figure 2 | XRD analysis of NSC: (a) XRD patterns of NSC before adsorption; (b) XRD patterns of NSC after adsorption at initial pH of 5.5.

40–70 nm. Figure 2(a) is X-ray diffraction pattern of NSC before adsorption. Diffraction peaks were observed at 2Theta = 29.400, 35.968, 39.408, 43.157, 47.505 and 48.503 which were corresponding to 104, 110, 11-3, 202, 018 and 11-6 planes, respectively, marching calcite crystal of $CaCO_3$ (PDF#47-1743). Those diffraction peaks could also be observed after phosphorus removal. Also, new peaks at 2Theta = 25.951, 31.503 and 32.187 shown in Figure 2(b) were corresponding to 002, 330 and −202 planes, respectively, which belonged to lattice planes of $Ca_{10}(PO_4)_6CO_3$ (PDF#35-0180). The generation of new crystals inferred chemical adsorption in solution. Adsorbed solution was dilute in different concentrations and tested by ICP. None Al^{3+}, Fe^{3+} and other impurity ions appeared in the solution, which suggested that NSC will not bring harmful impurities to aqueous solution.

The RSM design for adsorption studies

The statistical analysis

The solution temperature, contact times, initial pH and adsorbent dosage were chosen as the independent variables based on previous experiments (Choi *et al.* 2016; Yu *et al.* 2017; Zhang *et al.* 2018), while the adsorption rate as the response. Box-Behnken Design was conducted as experiment method. Twenty-five kinds of experimental combinations were designed in the experiment. In order to reduce the error, the center point was repeated five times. Therefore, a total of 29 experimental runs were carried out and the experimental scheme and results are listed in Table 2.

Quadratic polynomial of response surface was established as Equation (4) to fit experimental results:

$$\begin{aligned} Y = & -383.73508 + 0.43413X_1 + 7.98333X_2 \\ & + 109.241X_3 + 0.63314X_4 + 0.007X_1X_2 + 0.188X_1X_3 \\ & + 0.00443X_1X_4 - 1.71X_2X_3 - 0.0019X_2X_4 \\ & - 0.0104X_3X_4 - 0.033527X_1^2 + 0.13058X_2^2 \\ & - 8.92767X_3^2 - 0.000964267X_4^2 \end{aligned} \quad (4)$$

The determination coefficient and residuals of analysis of variance (ANOVA) were used as criterions to check the statistical adequacy of the model. According to the analysis software (Design Expert V8.0), the model has high values of the determination coefficient ($R^2 = 0.9658$) and the adjusted determination coefficient ($R^2_{adj} = 0.9315$), which meant that only 3.42% of the total variation is not explained by the regression model and the model parameters were significant (Shojaeimehr *et al.* 2014). The results of ANOVA were presented in Table 3. The low probability ($p < 0.05$) with F value (28.22) implied that the model predicted the adsorption rate of phosphorus appropriately. Moreover, the insignificant lack of fit ($p = 0.1151 > 0.05$) suggested that it is not significantly relative to the pure error and, thus, Equation (4) and the model were accurate for the experiment (Asfaram *et al.* 2015). The significance of the parameter coefficients, the associated standard error, and the effect of each terms in Equation (4) are also presented in Table 3. According to p values (<0.05 is significant), it can be obtained that all the first-order main effects are highly significant. In the quadratic term, temperature and adsorption dosage (X_1X_4), contact times and initial pH

Table 2 | Factors, levels and date of Box-Behnken design

Variables	Code	Level of factors		
		−1	0	1
Temperature (°C)	X_1	35	40	45
Contact time (h)	X_2	9	10	11
Initial pH	X_3	5	5.5	6
Adsorbent dosage (mg/L)	X_4	300	350	400

Run	Coded levels				Adsorption rate (%)
	X_1	X_2	X_3	X_4	
1	35	10	5.5	400	89.33
2	45	9	5.5	350	92.76
3	40	9	5.5	400	93.24
4	40	10	5.5	350	93.33
5	40	10	6.0	300	84.43
6	40	9	5.0	350	90.71
7	40	11	5.5	300	87.46
8	45	10	5.5	300	87.85
9	45	10	5.0	350	91.59
10	35	9	5.5	350	87.74
11	40	10	6.0	400	89.47
12	40	10	5.0	300	85.23
13	40	11	5.5	400	93.78
14	40	11	5.0	350	93.93
15	35	11	5.5	350	90.26
16	40	10	5.5	350	92.13
17	45	10	5.5	400	95.74
18	45	11	5.5	350	95.42
19	40	10	5.5	350	92.57
20	35	10	5.5	300	85.87
21	35	10	5.0	350	89.62
22	40	10	5.0	400	91.31
23	40	10	5.5	350	92.23
24	35	10	6.0	350	86.40
25	40	10	5.5	350	92.63
26	40	9	5.5	300	86.54
27	40	11	6.0	350	89.27
28	45	10	6.0	350	90.25
29	40	9	6.0	350	89.47

(X_2X_3), quadratic temperature (X_1^2), quadratic initial pH (X_3^2) and quadratic adsorption dosage (X_4^2) show high significant effects. Other variables have non-significant effect on phosphorus removal due to high p values.

Table 3 | ANOVA for response surface quadratic model

Source	Sum of squares	df	Mean square	*F*-value	*P*-value
Model	250.10	14	17.86	28.22	<0.0001
X_1	49.57	1	49.57	78.30	<0.0001
X_2	7.78	1	7.78	12.28	0.0035
X_3	14.30	1	14.30	22.59	0.0003
X_4	104.96	1	104.96	165.78	<0.0001
X_1X_2	4.90E-03	1	4.90E-03	7.74E-03	0.9311
X_1X_3	0.88	1	0.88	1.40	0.2571
X_1X_4	4.91	1	4.91	7.75	0.0146
X_2X_3	2.92	1	2.92	4.62	0.0496
X_2X_4	0.04	1	0.04	0.06	0.8147
X_3X_4	0.27	1	0.27	0.43	0.5240
X_1^2	4.56	1	4.56	7.20	0.0178
X_2^2	0.11	1	0.11	0.17	0.6823
X_3^2	32.31	1	32.31	51.04	<0.0001
X_4^2	37.70	1	37.70	59.54	<0.0001
Residual	8.86	14	0.63		
Lack of fit	7.97	10	0.80	3.58	0.1151
Pure error	0.89	4	0.22		
Cor total	258.96	28			

The optimization of adsorption process

In order to optimize the optimum conditions for phosphorus adsorption, it was necessary to study the effect of each variable on the adsorption efficiency. According to the results of the Box-Behnken Design, the factors with significant interaction effects were selected and the three dimensional response surface plots were drawn for investigation. Figure 3(a) shows the simultaneous effect of temperature and dosage of adsorbent on phosphorus adsorption rate (X_1X_4) when the other factors were maintained in the constant value. In constant adsorbent dosage, phosphorus adsorption rate increases with temperature increasing. This phenomenon may be due to the promotion of the molecules movement and ion diffusion (Zhang *et al.* 2018) at high temperature. The dosage of adsorbent extremely influenced the amount of adsorption. At a stable temperature, the adsorption rate enhances with the increase of the dosage of adsorbent which is likely to be the consequence of the greater amount of surface area and available binding sites on the surface of the adsorbent with the addition of NSC (Wang *et al.* 2014). However, when the dosage of adsorbent continues to be raised, the adsorption rate increases very slowly, and the dosage exceeds 375 mg/L, the adsorption rate remains

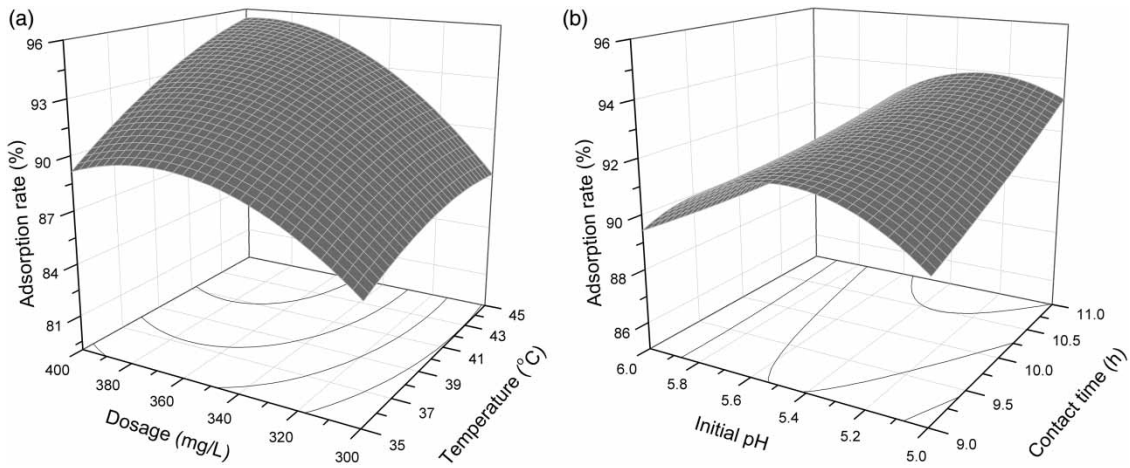

Figure 3 | 3D diagrams of significant interactions: (a) the effect of temperature and adsorbent dosage on phosphorus adsorption rate of NSC; (b) the effect of initial pH and contact time on phosphorus adsorption rate of NSC.

basically unchanged. In other words, the adsorption capacity is increased first and then reduced. Too many adsorbents brought out unsaturation of the active sites during the adsorption process is one of the principles (Liu *et al.* 2011). Also, an opposite presumption is that particle aggregation phenomenon can cause the decrease of the total surface active sites (Shojaeimehr *et al.* 2014).

The effect of the contact time and initial pH is shown in Figure 3(b). The phosphorus adsorption rate increased slightly with the increasing of the contact times. This may be due to the fact that when the contact time reaches 9 h, the solution is close to equilibrium, and the driving force for the adsorption of phosphorus by NSC is too weak to overcome the mass transfer resistance against phosphorus diffusion from bulk to surface active sites gradually (Jiang *et al.* 2014). $CaCO_3$ has ionization and hydrolysis situations in the solution and shown in Equations (5) and (6). When the pH of phosphate solution is between 5 and 6, there will be HPO_4^{2-} and $H_2PO_4^-$ in the solution. The removal process of phosphorus can be described through Equations (7) and (8) (Liu *et al.* 2012). As the pH value increases, the concentration of the HPO_4^{2-} species increases (Wang *et al.* 2016). As a result, $CaHPO_4$ with lower solubility will be synthesized more indicated from Equation (8). This may be the reason for the increase of phosphorus adsorption rate when the pH increases from 5 to 5.5 shown in Figure 3(b). However, Equations (7) and (8) suggested that excessive pH can prevent $CaCO_3$ from ionizing and reduce the amount of calcium ions, thereby preventing phosphorus adsorption. This is the conjecture of the decreasing adsorption rate, when the pH is over 5.5. By using of the response surface design and optimization, the optimum adsorption rate (97.05%) was obtained at temperature of 45 °C, pH 5.3, adsorption time of 11 h, and absorbent amount of 392 mg/L. Under the identical conditions, the adsorption rate of normal $CaCO_3$ (AR), purchased from Sinopharm Chemical Reagent Co., Ltd, was only 45.41%, while that of NSC was 97.05%. However, when adsorption time was prolonged to more than 48 h, the adsorption rate of normal $CaCO_3$ could exceed 96%. The results showed that NSC had the ability to achieve the equilibrium state of adsorption faster than normal $CaCO_3$ and improve the efficiency of adsorption, but there was no significant difference in adsorption capacity between NSC and normal $CaCO_3$. On the one hand, the phenomenon may be due to the fact that the nanometer size makes the dissolution rate of NSC much faster than that of normal $CaCO_3$, so more Ca^{2+} are released per unit time and bound to P in the solution to achieve adsorption effect, but on the other hand, the total ionization or solubility of $CaCO_3$ will not be affected by the rate, so the final equilibrium state of phosphorus between the adsorbent and the solution will not change significantly, and the adsorption capacity of normal $CaCO_3$ is basically the same with NSC.

$$CaCO_3 = Ca^{2+} + CO_3^{2-} \quad (5)$$

$$CO_3^{2-} + H_2O = HCO_3^- + OH^- \quad (6)$$

$$Ca^{2+} + H_2PO_4^- = CaH_2PO_4^+ \quad (7)$$

$$Ca^{2+} + HPO_4^{2-} = CaHPO_4 \quad (8)$$

Adsorption kinetics

Adsorption kinetics describes the rate at which solutes are adsorbed and provides a reference for the sorption mechanism (Gu *et al.* 2016; Zolgharnein *et al.* 2017). The pseudo-first-order and pseudo-second-order kinetic models were commonly used for batch adsorption process and the models can be described as Equations (9) and (10). Where q_e and q_t are adsorption capacities (mg phosphorus/g NSC) at equilibrium and time t (h), respectively; k_1 is pseudo-first-order rate constant (h^{-1}); and k_2 is pseudo-second-order rate constant (g mg^{-1} h^{-1}).

$$\ln(q_e - q_t) = \ln q_e - k_1 t \quad (9)$$

$$t/q_t = t/q_e + 1/(k_2 q_e^2) \quad (10)$$

However, both the common kinetic models described the sorption process inaccurately with low determination coefficients ($R_1^2 = 0.849$, $R_2^2 = 0.542$). Figure 4(a) suggests that experimental data of 'time versus adsorption rate' curves was a shape of 'S'. Thus, logistic model was used to describe the curves. Equations (11) and (12) are the logistic growth model differential and integral form, respectively (Mindell *et al.* 1987). The logistic model is usually used to describe growth or diffusion with a limiting factor. In this study, N_t is the adsorption rate of phosphorus at time t (h), K is maximum theoretical adsorption rate, considered as 100%, r and a are constants and r represents the maximum ability to the increase of adsorption rate.

$$dN_t/dt = rN_t(K - N_t)/K \quad (11)$$

$$N_t = K/[1 + \exp(a - rt)] \quad (12)$$

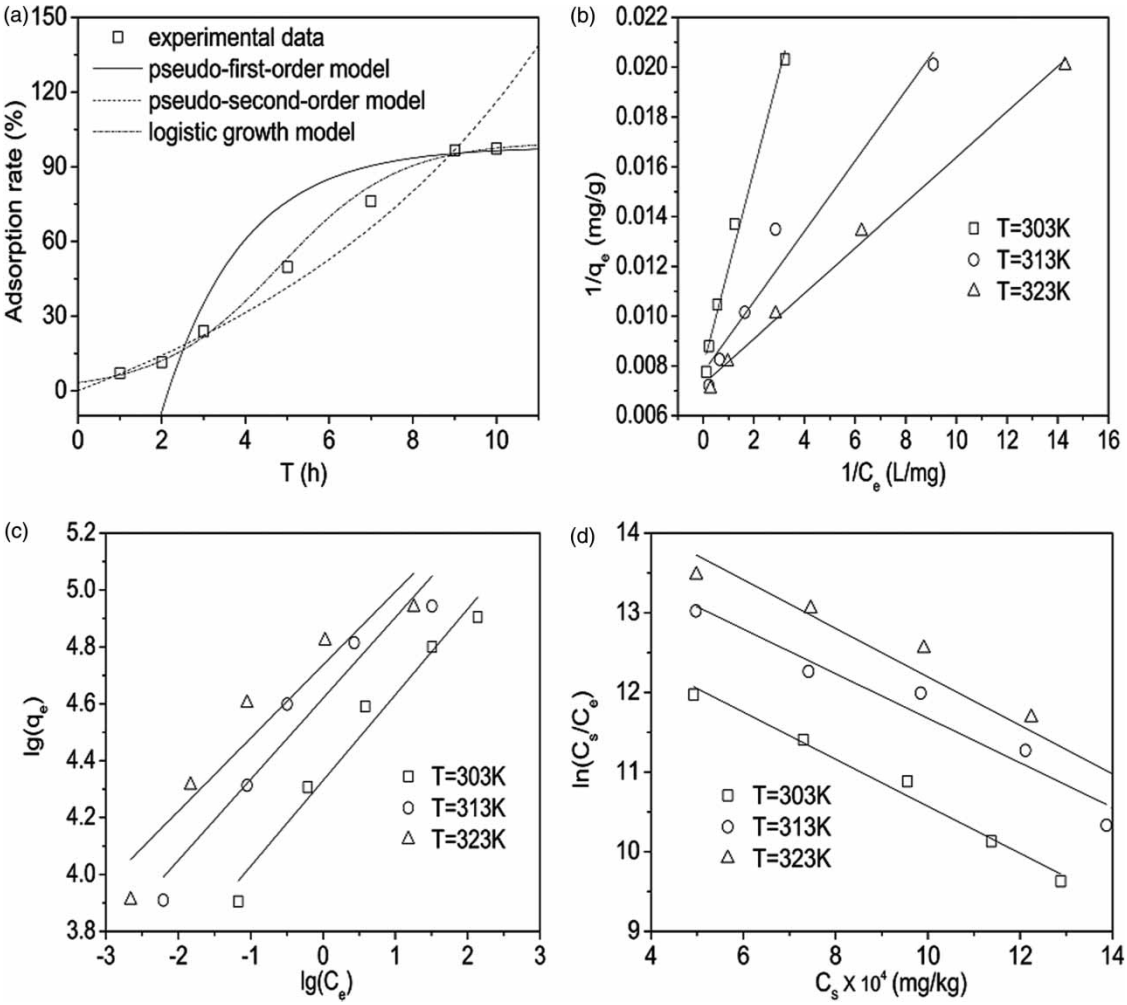

Figure 4 | The fitting of isotherm, kinetics and thermodynamics relevant parameters: (a) experimental data and calculated kinetic equation; (b) Langmuir isotherm of phosphorus adsorption at different temperatures; (c) Freundlich isotherm of phosphorus adsorption at different temperatures; (d) $\ln(C_s/C_e)$ versus C_s curve on adsorption of phosphorus at different temperatures.

Figure 4(a) shows that the logistic model predicted the adsorption rate accurately. Meanwhile, the remarkable determination coefficient ($R_3^2 = 0.986$) suggested the logistic model is the effective model for describing the process of phosphate removal by NSC. The values of parameters a and r were 3.381 and 0.699, respectively. The logistic growth equation was obtained as in Equation (13):

$$N_t = K/\left[1 + \exp\left(3.381 - 0.699t\right)\right] \tag{13}$$

According to Equations (5)–(8), the following facts can be inferred. The pH value of the solution increased with the increase of the adsorption time, which formed more phosphate precipitates and promoted the ionization of $CaCO_3$ in the previous hours. Thus, increment speed of adsorption rate was getting faster and faster. However, when the alkalinity of the solution was further increased, the ionization of calcium carbonate would be inhibited. Meanwhile, reduction of phosphorus concentration in solution led to the decrease of adsorption driving force. Both reduced the growth rate of adsorption and eventually achieved equilibrium. The final pH was 8.1 and the compound transformed from phosphate to $Ca_{10}(PO_4)_6CO_3$ shown in Figure 2(b).

Adsorption isotherm

At constant temperature, there is a mathematical relationship between the adsorption amount of adsorbent (q_e) and the equilibrium concentration of solute in solution (C_e). The models used to describe the equilibrium relationship is the adsorption isotherms. Differences in isotherm models are considered to be related to heterogeneity or homogeneity of the solid surface, the type of coverage, and the possibility of interaction between the adsorbate species (Tofik *et al.* 2016). Langmuir and Freundlich isotherms were the common models to analyze the adsorption of phosphorus in solution. The Langmuir and Freundlich model can be expressed as Equations (14) and (15). Where q_e (mg/g) is the equilibrium adsorption amount of absorbent, C_e (mg/L) is the equilibrium phosphorus concentration in the solution, and q_{max} (mg/g) is the maximum adsorption capacity of sorbent. q_{max} demonstrates the maximum amount of the adsorption capacity for the sorbent based on a monolayer coverage of adsorbate that is fully covered the sorbent homogeneous surface. K_a (L/mg) is the Langmuir constant related to adsorption energy. K_b and $1/n$ are the Freundlich constants:

$$C_e/q_e = C_e/q_{max} + 1/(K_a q_{max}) \tag{14}$$

$$\ln q_e = \ln K_b + (\ln C_e)/n \tag{15}$$

The Langmuir and Freundlich isotherms at different temperatures were fitted in Figure 4(b) and 4(c), respectively. The calculated parameters of the equations for different experimental systems are listed in Table 4. The determination coefficients of Langmuir are higher than those of Freundlich at the temperatures of 303 K, 313 K and 323 K, which indicates that adsorbent may have homogeneous surfaces and monolayer adsorption (Liu *et al.* 2016). Moreover, when the temperature rises from 303 K to 323 K, the maximum adsorption capacity estimated by isotherm increases from 123.844 mg/g to 137.552 mg/g, thus, heating is beneficial to the increase of adsorption capacity and this phenomenon is consistent with the result of response surface experiment.

Adsorption thermodynamics

Valuable data can be provided for the study of adsorption characteristics by adsorption thermodynamic research. The sign and magnitude of thermodynamic parameters, i.e. ΔH°, ΔS° and ΔG° are concerned with the feasibility and spontaneity nature of adsorption process and the relationship of parameters can be described as Equations

Table 4 | The Langmuir, Freundlich and thermodynamic model parameters at different temperatures

	Temperature (K)		
Parameter	**303**	**313**	**323**
Langmuir			
q_{max} (mg/g)	124.844	128.866	137.552
K_a (L/mg)	2.043	5.504	7.969
R^2	0.981	0.950	0.994
Freundlich			
K_b	75.966	101.401	114.033
n	3.317	3.512	3.890
R^2	0.961	0.927	0.881
Thermodynamics			
$\ln K_0$	13.528	14.473	15.241
ΔG° (kJ/mol)	−34.079	−37.663	−40.929
ΔH° (kJ/mol)	69.760		
ΔS° (kJ mol^{-1} K^{-1})	0.343		

(16)–(19) (Rawat *et al.* 1996; Tofik *et al.* 2016; Zolgharnein *et al.* 2017). Where ΔG° (kJ/mol) is standard free energy change, ΔH° (kJ/mol) is standard enthalpy change, ΔS° (kJ mol^{-1} K^{-1}) is standard entropy change, R (8.314 J mol^{-1} K^{-1}) is universal gas constant, T (K) is temperature, ΔH° and ΔS° are slope and intercept of the linear relationship of $\ln K_0$ versus $1/T$. C_s (mg/kg) is the quality of phosphorus in unit mass adsorbents, C_e (mg/L) is the equilibrium phosphorus concentration in the solution and K_0 is dimensionless equilibrium constant.

$$\Delta G^\circ = -RT \ln K_0 \tag{16}$$

$$\Delta G^\circ = \Delta H^\circ - T\Delta S^\circ \tag{17}$$

$$K_0 = \lim_{C_s \to 0} (C_S/C_e) \tag{18}$$

$$\ln K_0 = \Delta S^\circ/R - \Delta H^\circ/(RT) \tag{19}$$

According to Equation (18), K_0 can be obtained by plotting $\ln(C_s/C_e)$ versus C_s and extrapolating to zero C_s (Rawat *et al.* 1996). The intercept is the value of $\ln K_0$. Different temperatures were studied in Figure 4(d) and the results were listed in Table 4. The value of ΔG° is −34.079 kJ/mol, −37.663 kJ/mol and −40.929 kJ/mol at 303 K, 313 K and 323 K, respectively, ranges from −18 to −45 kJ/mol mean the coexistence of physical and chemical spontaneous adsorption. The positive value of ΔH° indicates an endothermic process, and the value of ΔH° is 69.760 > 40 kJ/mol which confirms that the adsorption of phosphorus by NSC is monolayer and mainly chemical adsorption (Emeniru *et al.* 2015), which corresponds with results of XRD. Meanwhile, with the positive value of ΔS° the randomness at the solid–liquid interface increases after adsorption (Gu *et al.* 2016). The adsorption capacity of NSC was compared with other sorbents in Table 5, which indicated NSC has a good ability to absorb phosphorus in an aqueous solution.

Table 5 | The comparison of the adsorption capacity between NSC and other kinds of sorbents

Sorbent	Adsorption capacity to P (mg/g)
NSC	123.79
Lanthanum-doped ordered mesoporous hollow silica spheres (Huang *et al.* 2014)	47.89
Fe-Al binary oxide (Tofik *et al.* 2016)	16.4
Cobalt hydroxide nanoparticles (Zolgharnein *et al.* 2017)	49.25
Calcium decorated sludge carbon (Kong *et al.* 2018)	116.82
nano-CaO_2-coated clinoptilolite (Zhou *et al.* 2017)	50.25

CONCLUSIONS

Box-Behnken Design of RSM model ($R^2 = 0.9658$) can accurately describe the adsorption of NSC on phosphorus in aqueous solution. When the phosphorus-P was 50 mg/L, the optimal adsorption rate ($R = 97.05\%$) of RSM prediction were at the condition of temperature of 45 °C, initial pH 5.3, contact time of 11 h and absorbent amount of 392 mg/L. Corresponding adsorption capacity was 123.79 mg/g. Compared with normal calcium carbonate, NSC can achieve adsorption equilibrium faster, but the adsorption capacity is not changed significantly.

Different from the general adsorption kinetics, the curve of adsorption rate with the change of time showed a type of 'S' which fitted with a logistic growth model. It is presumed that the adsorption is divided into two steps: the precipitation of $CaHPO_4$ is formed first, and with the increase of pH, the precipitation finally turns to $Ca_{10}(PO_4)_6CO_3$.

Langmuir isotherm showed better agreement with the adsorption than Freundlich isotherm. The thermodynamic studies proved that phosphorus removal by nano spherical $CaCO_3$ was a spontaneous, endothermic, random and mainly chemical adsorption process.

ACKNOWLEDGEMENT

This work was supported by the National Science Foundation of China (51425802).

CONFLICT OF INTEREST

The authors declare that they have no conflict of interest.

REFERENCES

Ahmad, T., Ahmad, K. & Alam, M. 2016 Sustainable management of water treatment sludge through '3R' concept. *Journal of Cleaner Production* **124**, 1–13.

Asfaram, A., Ghaedi, M., Hajati, S., Rezaeinejad, M., Goudarzi, A. & Purkait, M. K. 2015 Rapid removal of auramine-O and methylene blue by ZnS: Cu nanoparticles loaded on activated carbon: a response surface methodology approach. *Journal of the Taiwan Institute of Chemical Engineers* **53**, 80–91.

Cheng, H. & Xie, L. 2008 Study on the removal of phosphate in aqueous solution by nano calcium carbonate. *Industrial Safety and Environmental Protection* **34** (4), 17–19.

Choi, J., Chung, J., Lee, W. & Kim, J. O. 2016 Phosphorous adsorption on synthesized magnetite in wastewater. *Journal of Industrial and Engineering Chemistry* **34**, 198–203.

Diamadopoulos, E., Megalou, K., Georgiou, M. & Gizgis, N. 2007 Coagulation and precipitation as post-treatment of anaerobically treated primary municipal wastewater. *Water Environment Research* **79** (2), 131–139.

Emeniru, D. C., Onukwuli, O. D., DouyeWodu, P. E. & Okoro, B. I. 2015 The equilibrium and thermodynamics of methylene blue uptake onto ekowe clay; influence of acid activation and calcination. *International Journal of Engineering and Applied Sciences* **2** (5), 17–25.

Fang, W. M. & Shen, F. L. 2002 Influence of technological conditions on crystal shape and aggregate state of nano-particles of precipitated calcium carbonate in liquid phase. *Journal of Zhejiang University (Science Edition)* **29** (4), 437–441.

Gu, W., Xie, Q., Qi, C., Zhao, L. & Wu, D. 2016 Phosphate removal using zinc ferrite synthesized through a facile solvothermal technique. *Powder Technology* **301**, 723–729.

Huang, W., Zhu, Y., Tang, J., Yu, X., Wang, X., Li, D. & Zhang, Y. 2014 Lanthanum-doped ordered mesoporous hollow silica spheres as novel adsorbents for efficient phosphate removal. *Journal of Materials Chemistry A* **2** (23), 8839–8848.

Jiang, C., Jia, L., Zhang, B., He, Y. & Kirumba, G. 2014 Comparison of quartz sand, anthracite, shale and biological ceramsite for adsorptive removal of phosphorus from aqueous solution. *Journal of Environmental Sciences* **26** (2), 466–477.

Ko, Y. G., Do, T., Chun, Y., Kim, C. H., Choi, U. S. & Kim, J. Y. 2016 CeO_2-covered nanofiber for highly efficient removal of phosphorus from aqueous solution. *Journal of Hazardous Materials* **307**, 91–98.

Kong, L., Han, M., Shih, K., Su, M., Diao, Z., Long, J., Chen, D., Hou, L. & Peng, Y. 2018 Nano-rod Ca-decorated sludge derived carbon for removal of phosphorus. *Environmental Pollution* **233**, 698–705.

Liu, J., Wan, L., Zhang, L. & Zhou, Q. 2011 Effect of pH, ionic strength, and temperature on the phosphate adsorption onto lanthanum-doped activated carbon fiber. *Journal of Colloid and Interface Science* **364** (2), 490–496.

Liu, Y., Sheng, X., Dong, Y. & Ma, Y. 2012 Removal of high-concentration phosphate by calcite: effect of sulfate and pH. *Desalination* **289**, 66–71.

Liu, S. B., Tan, X. F., Liu, Y. G., Gu, Y. L., Zeng, G. M., Hu, X. J., Wang, H., Zhou, L., Jiang, L. H. & Zhao, B. B. 2016 Production of biochars from Ca impregnated ramie biomass (*Boehmeria nivea* (L.) Gaud.) and their phosphate removal potential. *RSC Advances* **6** (7), 5871–5880.

Mindell, D. P., Albuquerque, J. L. B. & White, C. M. 1987 Breeding population fluctuations in some raptors. *Oecologia* **72** (3), 382–388.

Oladoja, N. A., Adelagun, R. O. A., Ololade, I. A., Anthony, E. T. & Alfred, M. O. 2014 Synthesis of nano-sized hydrocalumite from a gastropod shell for aqua system phosphate removal. *Separation and Purification Technology* **124**, 186–194.

Rawat, J. P., Iraqi, S. U. & Singh, R. P. 1996 Sorption equilibria of cobalt (II) on two types of Indian soils – the natural ion exchangers. *Colloids and Surfaces A: Physicochemical and Engineering Aspects* **117** (1–2), 183–188.

Shojaeimehr, T., Rahimpour, F., Khadivi, M. A. & Sadeghi, M. 2014 A modeling study by response surface methodology (RSM) and artificial neural network (ANN) on Cu^{2+} adsorption optimization using light expended clay aggregate (LECA). *Journal of Industrial and Engineering Chemistry* **20** (3), 870–880.

Somasundaran, P. & Agar, G. E. 1967 The zero point of charge of calcite. *Journal of Colloid and Interface Science* **24** (4), 433–440.

Tofik, A. S., Taddesse, A. M., Tesfahun, K. T. & Girma, G. G. 2016 Fe–Al binary oxide nanosorbent: synthesis, characterization and phosphate sorption property. *Journal of Environmental Chemical Engineering* **4** (2), 2458–2468.

Wang, J., Lin, X., Luo, X. & Long, Y. 2014 A sorbent of carboxymethyl cellulose loaded with zirconium for the removal of fluoride from aqueous solution. *Chemical Engineering Journal* **252**, 415–422.

Wang, Y., Yu, Y., Li, H. & Shen, C. 2016 Comparison study of phosphorus adsorption on different waste solids: fly ash, red mud and ferric–alum water treatment residues. *Journal of Environmental Sciences* **50**, 79–86.

Yu, Z., Zhang, C., Zheng, Z., Hu, L., Li, X., Yang, Z., Ma, C. & Zeng, G. 2017 Enhancing phosphate adsorption capacity of SDS-based magnetite by surface modification of citric acid. *Applied Surface Science* **403**, 413–425.

Zhang, X., Lin, X., He, Y., Chen, Y., Zhou, J. & Luo, X. 2018 Adsorption of phosphorus from slaughterhouse wastewater by carboxymethyl konjac glucomannan loaded with lanthanum. *International Journal of Biological Macromolecules* **119**, 105–115.

Zhou, K., Wu, B., Su, L., Gao, X., Chai, X. & Dai, X. 2017 Development of nano-CaO_2-coated clinoptilolite for enhanced phosphorus adsorption and simultaneous removal of COD and nitrogen from sewage. *Chemical Engineering Journal* **328**, 35–43.

Zolgharnein, J., Dalvand, K., Rastgordani, M. & Zolgharnein, P. 2017 Adsorptive removal of phosphate using nano cobalt hydroxide as a sorbent from aqueous solution; multivariate optimization and adsorption characterization. *Journal of Alloys and Compounds* **725**, 1006–1017.

First received 21 October 2018; accepted in revised form 21 January 2019. Available online 29 January 2019